Confinement transition of $\mathbb{Z}_2$ gauge theories coupled to massless fermions: Emergent quantum chromodynamics and *SO*(5) symmetry

Snir Gazit[a,1], Fakher F. Assaad[b], Subir Sachdev[c,d,1], Ashvin Vishwanath[c], and Chong Wang[c]

[a]Department of Physics, University of California, Berkeley, CA 94720; [b]Institut für Theoretische Physik und Astrophysik, Universität Würzburg, 97074 Würzburg, Germany; [c]Department of Physics, Harvard University, Cambridge MA 02138; and [d]Perimeter Institute for Theoretical Physics, Waterloo, ON, Canada N2L 2Y5

Contributed by Subir Sachdev, June 8, 2018 (sent for review April 12, 2018; reviewed by Shailesh Chandrasekharan and Ribhu Kaul)

We study a model of fermions on the square lattice at half-filling coupled to an Ising gauge theory that was recently shown in Monte Carlo simulations to exhibit $\mathbb{Z}_2$ topological order and massless Dirac fermion excitations. On tuning parameters, a confining phase with broken symmetry (an antiferromagnet in one choice of Hamiltonian) was also established, and the transition between these phases was found to be continuous, with coincident onset of symmetry breaking and confinement. While the confinement transition in pure gauge theories is well-understood in terms of condensing magnetic flux excitations, the same transition in the presence of gapless fermions is a challenging problem owing to the statistical interactions between fermions and the condensing flux excitations. The conventional scenario then proceeds via a two-step transition, involving a symmetry-breaking transition leading to gapped fermions followed by confinement. In contrast, here, using quantum Monte Carlo simulations, we provide further evidence for a direct, continuous transition and also find numerical evidence for an enlarged *SO*(5) symmetry rotating between antiferromagnetism and valence bond solid orders proximate to criticality. Guided by our numerical finding, we develop a field theory description of the direct transition involving an emergent nonabelian [*SU*(2)] gauge theory and a matrix Higgs field. We contrast our results with the conventional Gross–Neveu–Yukawa transition.

fractionalization | confinement | deconfined criticality | emergent symmetry | antiferromagnetism

Classical and quantum phase transitions have traditionally been studied in the framework of the Landau–Ginzburg–Wilson (LGW) paradigm. Phases are distinguished on the basis of whether they preserve or break global symmetries of the Hamiltonian. Two distinct phases can be separated by a continuous phase transition only when one of them breaks a single symmetry, which is preserved in the other.

More recently, studies of correlated quantum systems have led to many examples of important physical models displaying phase transitions that do not fit this familiar paradigm. We can have continuous quantum phase transitions between phases that break distinct symmetries (1). On allowing for topological order, several new types of quantum phase transitions become possible. We can have continuous phase transitions between a phase with topological order and a phase without topological order, both of which preserve all symmetries: the earliest example of this is the phase transition in the Ising gauge theory in 2 + 1 dimensions described by Wegner (2). We can also have continuous quantum transitions between phases with distinct types of topological order, and many examples are known in fractional quantum Hall systems (3, 4). We can have a continuous transition from a phase with topological order to one with a broken symmetry (5–7). Finally, we can have phase transitions between a Dirac semimetal and various gapped states, including a symmetric gapped state without topological order dubbed symmetric mass generation (SMG) (8–13).

Theories of these transitions all involve quantum-field theories with deconfined emergent gauge fields. The presence of the gauge fields reflects the long-range quantum entanglement near the critical point: this entanglement is not easily captured by the symmetry-breaking degrees of freedom or their fluctuations. The gauge theories have varieties of Higgs and confining phases, and transitions between these phases allow for the transitions described above.

In this paper, we will present an example of a deconfined critical point between a deconfined phase with topological order and a confining phase with broken symmetry. The deconfined phase has Z_2 topological order, but in contrast to conventional topologically ordered states, which are gapped, it also features gapless fermionic excitations, with gaplessness that is protected by the symmetries of the underlying Hamiltonian. This is an example of a "nodal" Z_2 topological order that has been invoked in the context of the square lattice antiferromagnet (14) and in the Kitaev model on the honeycomb lattice (15). Here, we will augment the model to include both spin and charge conservation leading to a larger number of Dirac fermions (four flavors of complex two-component fields), which can be simulated without a sign problem. Thus, we will be studying how the confinement transition in a gauge theory is modified by the presence of gapless charged fermions.

Significance

Universal properties of quantum (zero-temperature) phase transitions are typically well-described by the classical Landau theory of spontaneous symmetry breaking. A paradigmatic counterexample is deconfined criticality, where quantum interference allows for a direct and continuous transition between states with distinct symmetry-breaking patterns, a phenomenon that is classically forbidden. In this work, we extend the scope of deconfined criticality to a case where breaking of a global symmetry coincides with confinement of a local (gauge) symmetry. Using Monte Carlo simulations, we investigate a lattice realization of this transition. Remarkably, we uncover emergent and enlarged global and gauge symmetries. These findings direct us in constructing a critical field theory description.

Author contributions: S.G., F.F.A., S.S., A.V., and C.W. performed research; S.G. and F.F.A. analyzed data; and S.G., F.F.A., S.S., A.V., and C.W. wrote the paper.

Reviewers: S.C., Duke University; and R.K., University of Kentucky.

The authors declare no conflict of interest.

[1]To whom correspondence may be addressed. Email: snirgaz@gmail.com or sachdev@g.harvard.edu.

This article contains supporting information online at www.pnas.org/lookup/suppl/doi:10.1073/pnas.1806338115/-/DCSupplemental.

Published online July 9, 2018.

The confining phase in the formulation used in our paper is an insulator on the square lattice at half-filling with two-sublattice antiferromagnetic (AFM) order, similar to that found in a cuprate compound like La_2CuO_4. The topologically ordered phase is also at half-filling. This phase can be considered as a toy model of a "pseudogap" phase relevant to the doped cuprate superconductors, although our analysis will be restricted to half-filling. We will argue that there is a direct transition between the insulating antiferromagnet and the phase with topological order and present a critical field theory with an emergent nonabelian $SU(2)$ gauge field.

Emergent symmetries will also play an important role in the analysis of our deconfined critical point. These are symmetries that are not present in the underlying Hamiltonian or in the noncritical phases but that become asymptotically exact at long distances and times in the critical regime. An emergent $SO(5)$ symmetry was proposed (16–18) for the deconfined critical point between the insulating AFM and valence bond solid (VBS) states on the square lattice: numerical computations on lattice models have observed such enhanced symmetries (19–23). We will present numerical evidence for the same $SO(5)$ symmetry between the AFM and VBS order parameters in our model. This emergent symmetry is intriguing, because neither of the two phases near the transition ["orthogonal semimetal" (OSM) or AFM] involve actual long-range VBS order, and yet, VBS fluctuations become as strong as AFM fluctuations at the critical point. As we shall see later, this feature arises naturally in our formulation of the critical theory.

We shall study a model introduced in recent quantum Monte Carlo (QMC) studies (24, 25). The model can be considered as an effective theory of electrons (c) on the square lattice. The model is expressed as an Ising lattice gauge theory (ILGT) coupled to "orthogonal" fermions (f). The QMC studies showed that this model exhibits a topological ordered OSM phase: this phase has a $\mathbb{Z}_2$ topological order and massless Dirac fermion excitations that carry $\mathbb{Z}_2$ electric charges and also, the spin and electromagnetic charges of the underlying electrons (c). The charges carried by these fermions are identical to the "orthogonal fermions" introduced in ref. 26, and therefore, we have adopted their terminology. The previous studies also presented evidence for a confining AFM phase along with a possible direct and continuous phase transition between the OSM and AFM phases. However, the underlying mechanism of this transition was not understood.

Our QMC simulation finds numerical evidence for an emergent $SO(5)$ symmetry, rotating between AFM and VBS orders, at criticality. We contrast this finding with the more standard Gross–Neveu–Yukawa (GNY) universality class, where such an enlarged symmetry is absent. Guided by the numerical results, we conjecture that the critical theory describing the confinement transition is given by a two-color [$SU(2)$] quantum chromodynamics (QCD) with $N_f = 2$ flavors of Dirac fermions coupled to a near-critical matrix Higgs field. The Higgs mechanism is shown to naturally allow access to both the confined and deconfined phases using a single tuning parameter. The mechanism described here resembles the theory of SMG (12, 13) in some respects but differs in the representation of the Higgs field under the gauge group. While SMG required Higgs fields transforming in the fundamental representation and therefore, the Higgs phase was free of topological order, here we will use a Higgs field in the adjoint representation, and the Higgs phase will therefore inherit a $\mathbb{Z}_2$ topological order along with gapless fermions.

Model, Symmetries, and Phase Diagram

Model. We consider the Hamiltonian $\mathcal{H} = \mathcal{H}_{\mathbb{Z}_2} + \mathcal{H}_f$ illustrated in Fig. 1. The ILGT part of the Hamiltonian (2) reads

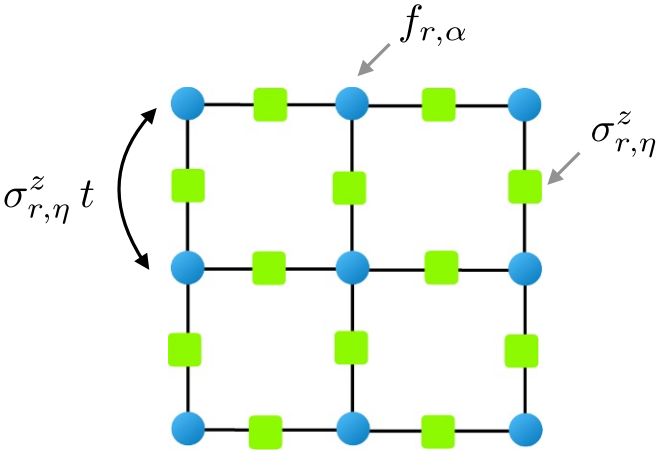

Fig. 1. Lattice model—the fermions $f_{r,\alpha}$ reside on the square lattice sites (blue circles), and the Ising gauge fields $\sigma^z_{r,\eta}$ reside on the bonds (green squares). The Ising gauge field determines the sign of the hopping amplitude along the corresponding bond.

$$\mathcal{H}_{\mathbb{Z}_2} = -J \sum_{\square} \prod_{b \in \square} \sigma^z_b - h \sum_b \sigma^x_b. \qquad [1]$$

Here, σ^z_b and σ^x_b are the conventional Pauli matrices, $\square$ labels the square lattice elementary plaquettes, and $b = \{r, \hat{\eta}\}$ denotes the square lattice bonds, with $r = \{r_x, r_y\}$ being the lattice site and $\hat{\eta} = \hat{x}/\hat{y}$. The fermionic part of the Hamiltonian is given by

$$\mathcal{H}_f = -t \sum_{r,\hat{\eta},\alpha} \sigma^z_{r,\hat{\eta}} f^\dagger_{r+\hat{\eta},\alpha} f_{r,\alpha} + \text{h.c.} + U \sum_r \left(n^\uparrow_r - \frac{1}{2}\right)\left(n^\downarrow_r - \frac{1}{2}\right), \qquad [2]$$

where h.c. denotes hermitian conjugate, the operator $f^\dagger_{r,\alpha}$ creates an orthogonal fermion (26) at site r with spin polarization α, and $n_r = \sum_\alpha f^\dagger_\alpha f_\alpha = n^\uparrow_r + n^\downarrow_r$ is the fermion density.

By itself, this model cannot be a complete representation of the spin and charge excitations of a lattice electron model, like the Hubbard model. This is because it is not possible to write down a gauge-invariant electron operator, c_r, in terms of the f_r and the $\sigma_{r,\hat{\eta}}$. We need another bosonic degree of freedom that carries a $\mathbb{Z}_2$ electric charge. We will introduce such a degree of freedom later in *Critical Theory of the Confinement Transition*, but for now, we assume that this boson is gapped in all of the phases that we study below; we will not include it in our numerical study of $\mathcal{H}$.

As we show below, by varying the strength of the onsite Hubbard interaction term, in Eq. **2**, we map a more generic phase diagram compared with the ones obtained in refs. 24 and 25. Furthermore, this extension allows us to test the stability of the OSM confinement transition and to compare its critical properties with the more standard GNY and three-dimensional classical Ising universality classes.

Symmetries. The global and local symmetries of the Hamiltonian will play an important role in our analysis. First, the Hamiltonian is invariant under global $SU_s(2)$ rotations corresponding to spin rotation symmetry. Second, because we restrict ourselves to half-filling, our model is also invariant under the particle hole (PH) transformation $f_\alpha \to (-1)^{r_x + r_y} f^\dagger_\alpha$. Third, combining PH symmetry with the $U_c(1)$ symmetry corresponding to particle number conservation forms an enlarged $SU_c(2)$ pseudospin symmetry rotating between charge density wave (CDW) and the Bardeen–Cooper–Schrieffer (BCS) superconducting order parameters (27).

Partial PH symmetry, acting only on one of the spin species, maps between the charge, n_r, and the spin, $S_r^z = n_r^\uparrow - n_r^\downarrow$, operators. Consequently, partial PH symmetry interchanges between the symmetries $SU_s(2)$ and $SU_c(2)$ and when these symmetries are broken, between AFM and BCS/CDW orders, respectively. The Hubbard term in Eq. **2** explicitly breaks partial PH symmetry, since under the symmetry action, repulsive interaction is mapped to attractive interaction, $U \to -U$ (28).

The correspondence of our model to lattice gauge theories (LGTs) is manifest in the extensive number of local Ising symmetries generated by the operators $G_r = (-1)^{n_r} \prod_{b\in+_r} \sigma_b^x$, with $+_r$ denoting the set of bonds emanating from the site r. The eigenvalues, $Q_r = \pm 1$, of G_r are conserved quantities and within the Hamiltonian formalism of LGT (29), are identified with the static background $\mathbb{Z}_2$ charge.

The Hilbert space then decomposes into a direct sum of subspaces labeled by the $\mathbb{Z}_2$ charge configuration Q_r and comprises quantum states that obey an Ising variant of Gauss' law $G_r = Q_r$. For a uniform charge configuration, we can distinguish between two possibilities: an even LGT, $Q = 1$, with no background charge and an odd LGT, $Q = -1$, with a single $\mathbb{Z}_2$ background charge at each site. We note that partial PH symmetry maps $Q \to -Q$.

Gauss's law can be explicitly enforced (25), or alternatively, it is generated dynamically at sufficiently low temperatures (24). In the numerical computation below, we will consider both options depending on numerical convenience. The zero-temperature universal properties of our model, which are the focus of this study, do not depend on the above choice.

Phase Diagram. We now determine the general structure of the zero-temperature phase diagram (Fig. 2*A*) by studying several limiting cases. For concreteness, we consider negative values of J (the case $J > 0$ is discussed in ref. 25) and set $-t = |J|$. All other energy scales are measured in units of $|J|$. We will only consider the odd LGT case, which as we explain, is compatible with repulsive Hubbard interactions, $U > 0$. The corresponding results for the even LGT can be easily obtained by applying a partial PH transformation with the appropriate identification of symmetries and order parameters as discussed above.

We first consider the strong coupling limit $h \gg t, U, |J|$. In the extreme limit $h \to \infty$, the ILGT ground state is given by the product state $|\Psi_{\text{conf}}^\sigma\rangle = \prod_b |\sigma_b^x = 1\rangle$ as follows directly from minimizing the transverse field term in Eq. **1**. In the above limit, we can safely neglect quantum fluctuations and substitute $\sigma_b^x = 1$ in the Ising Gauss's law. This yields the relation $Q_r = (-1)^{n_r}$, such that the local fermion parity, $(-1)^{n_f}$, becomes a conserved quantity identified with the background Ising charge, Q_r.

After the standard LGT analysis (29), we now establish the effective interaction between a pair of Ising charge excitations in the strong coupling limit. To comply with Ising Gauss's law, a string of flipped Ising gauge field, $\sigma_b^x = -1$, must connect any pair of Ising charges. The energy cost associated with each spin flip is proportional to h, and thus, the interaction potential grows linearly with the separation giving rise to confinement.

The repulsive Hubbard interaction favors single onsite occupancy and consequently, gaps even parity (doublons and holons) states. The resulting low-energy sector is an odd LGT with a emergent Gauss law constraint $G_r = -1$. This leaves the onsite fermion spin as the only remaining dynamical degree of freedom. Reintroducing quantum fluctuations, at large but finite transverse field h, allows for virtual hopping processes. Similar to the superexchange mechanism, such fluctuations induce an effective AFM Heisenberg interaction proportional to t^2/h. The zero-temperature ground state will then spontaneously break the spin rotational symmetry, $SU_s(2)$, by forming a Néel AFM state.

Next, we examine the weak coupling limit $J \gg t, h, U$. Here, minimizing the Ising flux term in Eq. **1** (for negative J) realizes a uniform π-flux state, $|\Psi_{\text{de-conf}}^\sigma\rangle = \prod_\square |\Phi_\square = -1\rangle$, where $\Phi_\square = \prod_{b\in\square} \sigma_b^z$ is the Ising flux threading the elementary plaquette, $\square$. Crucially, the single-particle spectrum of the π-flux lattice hosts a pair of gapless Dirac fermions (30). In the resulting phase, the matter fields are deconfined, since in contrast to the confining phase, gauge field fluctuations mediate only short-range attractive interaction with a vanishing string tension. The deconfined phase hosts fractionalized excitations carrying long-range entanglement (31). We note that a π-flux phase can be stabilized even if J is positive by taking the large-hopping amplitude t limit (24, 25).

The gapless deconfined phase resembles the well-known gapless $\mathbb{Z}_2$ spin liquid using the condensed matter theory parlance (14, 32). However, there is one crucial difference: in our case, the fermionic matter fields carry, in addition to the $SU(2)$ spin charge (similar to conventional spinons), an $U(1)$ electromagnetic charge. This makes our model more closely related to an orthogonal metal (OM) construction (26), where the fractionalization pattern involves decomposing the physical fermion into a product of a fermion carrying both spin and charge and an Ising spin. Both slave particles carry an Ising gauge charge. We, therefore, dub this phase OSM.

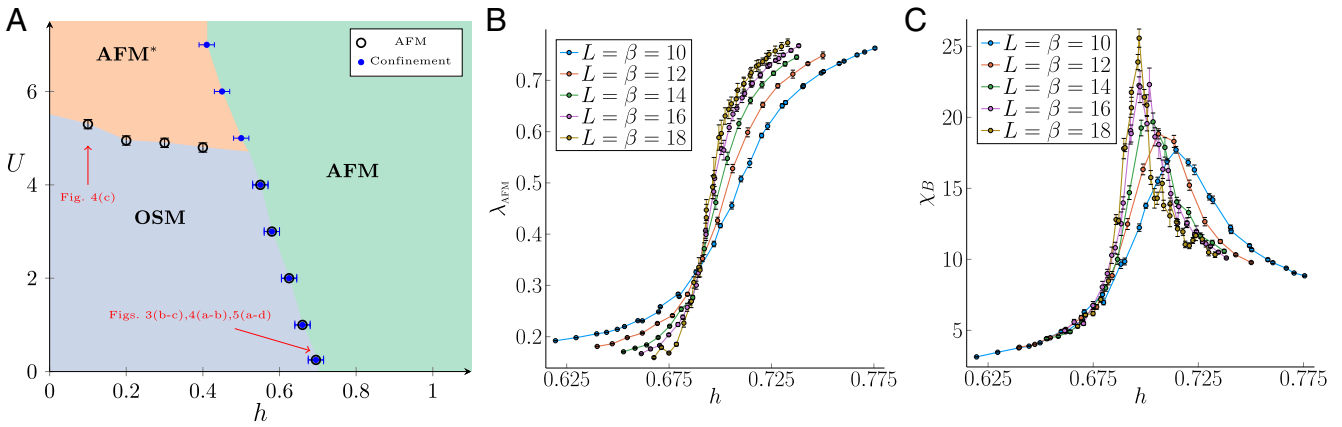

Fig. 2. (*A*) Phase diagram of the ILGT coupled to fermions. Red arrows point to parameter cuts studied in Figs. 3–5. (*B* and *C*) Simulation of the OSM confinement transition carried out at $U = 0.25$ as a function of h. (*B*) The onset of AFM order is located by a curve-crossing analysis of the susceptibility ratio λ_{AFM}, and (*C*) the confinement transition is located from the divergence of the Ising flux susceptibility, χ_B.

Due to the vanishing density of states at half-filling, the Dirac phase is stable against AFM order for weak Hubbard interactions, $U \ll t$. However, a transition to an AFM^* phase is expected at sufficiently large coupling. Here, the asterisk expresses the fact that the gauge theory remains deconfined in the AFM^* phase. This situation should be contrasted with the confined phase, where along with AFM symmetry-breaking order, the gauge sector is confined.

Phase Transitions. The different phases of our model are classified according to the presence or absence of topological order and conventional symmetry-breaking AFM order. Thus, the associated phase transitions are expected to involve confinement, symmetry breaking, or both.

More specifically, the phase transition between the deconfined Dirac phase and the AFM^* phase is solely marked by the rise of AFM order, while the Ising gauge field sector remains deconfined. Therefore, the transition belongs to the conventional chiral GNY universality class (33–36). However, across the transition between the confined AFM and AFM^* phases, the gapped fermions are only spectators, and the transition is signaled by the emergence of topological order in the AFM^* phase. Thus, the phase transition corresponds to the standard confinement transition of the pure Ising gauge theory, which belongs to the three-dimensional classical Ising model universality class [the spin-wave (Goldstone) modes are not expected to modify the universality class of this transition as can be seen in the methods of ref. 37].

The most interesting phase transition, which is the subject of this study, is between the deconfined Dirac phase and the confined AFM. Previous numerical simulations (24, 25) and the results shown below have found evidence for a single and continuous phase transition involving both symmetry breaking and confinement. Gaining a better analytic and numerical understanding of this transition is the main subject of the remainder of this paper.

QMC

Methods. The ILGT coupled to fermions is free of the numerical sign problem for arbitrary fermion density (here we are interested only in the half-filled case) (24, 25). This allows us to study our model using unbiased and numerically exact (up to statistical errors) QMC simulations. We use the standard auxiliary-field QMC algorithm (38, 39) using both single spin-flip updates and global moves inspired by the worm algorithm (25). In all cases, we set the imaginary time Trotter step to be $|t|\Delta\tau = 1/12$, a value for which the discretization errors are controlled. In what follows, we set $t = J = -1$ and explore the phase diagram as a function of h and U. Unless otherwise stated, we also explicitly impose Gauss's law constraint. Further technical details of our numerical scheme as well as additional numerical data can be found in *SI Appendix*.

Observables. We probe the VBS and AFM order parameters using the bond kinetic energy, $\mathbf{D}^{x/y}$, and the fermion spin, $\mathbf{S}^{\gamma}$, operators, respectively. Their corresponding lattice definitions at finite wave vector, q, are given by,

$$\begin{aligned}\mathbf{D}^{\eta}(q) &= \sum_{r,\alpha} e^{iq\cdot r}\left(\sigma^{z}_{r,\eta} f^{\dagger}_{r+\eta,\alpha} f_{r,\alpha} + \text{h.c.}\right)\\ \mathbf{S}^{\gamma}(q) &= \sum_{r,\alpha,\beta} e^{iq\cdot r} f^{\dagger}_{r,\alpha}\tau^{\gamma}_{\alpha\beta} f_{r,\beta}\end{aligned} \qquad [3]$$

where $\tau^{\gamma}_{\alpha\beta}$ are the usual Pauli matrices.

On the π-flux square lattice, the set of fermion bilinears appearing in Eq. **3** forms a five-component supervector that transforms as a fundamental under $SO(5)$ rotations. Within this formalism, the competition between AFM and VBS fluctuations is explicitly manifest (16, 17).

To study fluctuations, we use the imaginary time static susceptibility, which for a generic operator, $\mathcal{O}$, is defined by $\chi_{\mathcal{O}}(q) = \frac{1}{\beta L^2}\left\langle \left(\int_0^{\beta} d\tau\, \mathcal{O}(q,\tau)\right)^2 \right\rangle$. Here, expectation values are defined with respect to the thermal density matrix, $\beta = 1/T$ is the inverse temperature T, and L is the linear system size. The ordering wave vector associated with AFM (VBS) order (along the $\hat{x}/\hat{y}$ bonds) equals $G_{\mathrm{AFM(VBS)}} = \{\pi,\pi\}(\{\pi,0\}/\{0,\pi\})$.

To locate the onset of AFM order, we use the renormalization group (RG)-invariant ratio $\lambda_{AFM} = 1 - \frac{\chi_S(G_{AFM}-\Delta q)}{\chi_S(G_{AFM})}$, with $|\Delta q| = 2\pi/L$ being the smallest wave vector on our finite lattice. λ_{AFM} approaches unity deep in an AFM phase and vanishes when the symmetry is restored (40). For a continuous transition, curves of λ_{AFM} corresponding to different Euclidean space–time volumes are expected to cross at the critical coupling. Anticipating the emergence of strong VBS fluctuations at criticality, we also define the analogous RG ratio, $\lambda_{VBS} = 1 - \frac{\chi_D(G_{VBS}-\Delta q)}{\chi_D(G_{VBS})}$.

For pure lattice gauge theories, it is standard to probe confinement via the Polyakov loop (41). In the presence of matter fields, the Polyakov loop no longer sharply defines confinement due to charge screening. In principle, one can detect the rise of topological order by extracting the topological contribution to the entanglement entropy (42, 43) or by measuring the Fredenhagen–Marcu (44, 45) order parameter. However, such probes are difficult to reliably scale with system size in fermionic QMC simulations. In our analysis, we detect the thermodynamic singularity associated with the confinement transition by probing the expected divergence of the Ising flux susceptibility, $\chi_B = \partial\langle\Phi\rangle/\partial J$, with Φ being the Ising flux density defined above (25).

Numerical Results. Our first task is to determine numerically the phase diagram shown in Fig. 2*A*. We exemplify our analysis by studying the OSM confinement transition. For concreteness, we fix $U = 0.25$ and drive the transition by increasing the strength of the transverse field, h. In our finite-size scaling analysis, we consider linear system sizes up to $L = 18$. We further assume relativistic scaling and accordingly consider inverse temperatures that grow linearly with the system size, $\beta = L$.

In Fig. 2*B*, we track the evolution of λ_{AFM} as a function of h. We observe a clear curve crossing that varies very little with system size and strongly indicates a continuous transition. The crossing point marks the rise of AFM order and allows us to estimate the critical coupling, $h_c^{\mathrm{AFM}}(U = 0.25) = 0.69(2)$. Moving to the IGLT sector, in Fig. 2*C*, we depict the Ising flux susceptibility, χ_B, across the confinement transition. With increase in the system size, χ_B displays a progressively diverging and narrowing peak. We use the peak position to estimate the critical coupling of the confinement transition to be $h_c^{\mathrm{conf}} = 0.69(2)$. This value coincides, within the error bars, with the emergence of AFM order, found above, suggesting that symmetry breaking and confinement occur simultaneously.

We use a similar analysis to determine the rest of the phase boundaries appearing in Fig. 2*A*. We find that the critical confinement line separating the AFM and AFM^* phases meets with the AFM transition line separating the OSM and the AFM^* phases at a tricritical point. The two critical lines then merge into a single line corresponding to the OSM confinement transition.

We now test the emergence of enlarged symmetries in the OSM confinement transition. In the presence of an $SO(5)$ symmetry, the scaling dimension of the VBS and AFM order parameters must coincide (19). As a direct consequence, similar

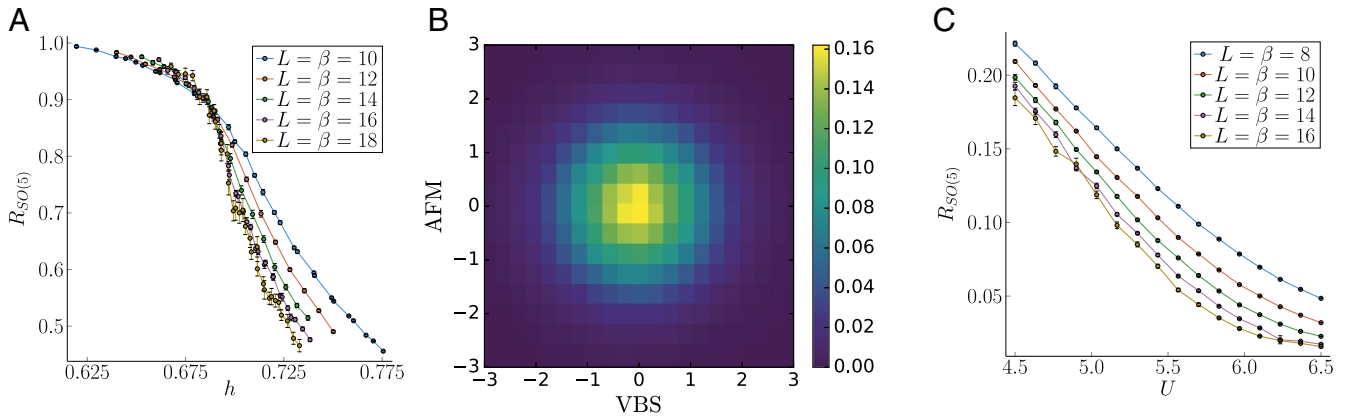

Fig. 3. Signature of an $SO(5)$ symmetry. (*A*) A clear curve crossing is observed in the susceptibility ratio $R_{SO(5)}$ across the OSM confinement transition for $U=0.25$ as a function of h. (*B*) Joint probability distribution $\mathbf{P}(D^x, \mathbf{S}^z)$ of the VBS and AFM order parameters at criticality. $\mathbf{P}(D^x, \mathbf{S}^z)$ exhibits a circular symmetry. (*C*) Susceptibility ratio $R_{SO(5)}$ across the AFM transition for $h=0.1$ as a function of U. The absence of curves crossing rules out the emergence of an $SO(5)$ symmetry at the GNY transition.

to λ_{AFM}, the susceptibilities ratio, $R_{SO(5)}=\chi_{\text{AFM}}(G_{\text{AFM}})/\chi_{\text{VBS}}(G_{\text{VBS}})$, becomes an RG invariant.

In Fig. 3*A*, we depict the susceptibility ratio, $R_{SO(5)}$, as a function of h across the confinement transition for different system sizes. Indeed, we find that all curves cross at a single point, independent of the space–time volume. We use the crossing point to pin down the critical coupling, $h_c^{SO(5)}=0.69(2)$, in excellent agreement with the above calculations using other observables. We note that this result is a necessary but not sufficient condition for the emergence of an $SO(5)$ symmetry. Nevertheless, it serves as a nontrivial test for this effect.

To further illustrate the emergence of an $SO(5)$ symmetry, in Fig. 3*B*, we depict a two-dimensional histogram approximating the joint probability distribution of the VBS and AFM order parameters at criticality. We note that, due to algorithmic limitations, in computing the AFM histogram one must simulate the constraint-free model. Doing so only slightly shifts the critical coupling, and as explained above, it does not affect critical properties. Remarkably, the joint distribution exhibits a circular form, which provides further indication for the emergence of an $SO(5)$ symmetry. We have also verified, using a similar analysis, that the joint probability distribution of the VBS order along the x and y directions affords an emergent, $SO(2)$, rotational symmetry at criticality (*SI Appendix*).

To better appreciate the above result, it is instructive to apply the susceptibility ratios analysis to the more conventional GNY transition. To that end, we investigate the transition between the OSM phase and the AFM* phase. We fix $h=0.1$ and cross the AFM transition by increasing U. The results of this analysis are shown in Fig. 3*C*. In stark contrast to the confinement transition, we find no evidence for a curve crossing. Thus, we can deduce that the putatively continuous OSM confinement transition must belong to a universality class that is distinct from the conventional GNY transition. This conclusion is one of our main results.

Motivated by the above results, we now extract the critical properties of the OSM confinement transition from the numerical data. The dimensionless susceptibility ratios are expected to follow a simple scaling form $\lambda_{\text{AFM/VBS}}(h,L)=\tilde{\lambda}_{\text{AFM/VBS}}(\delta h L^{1/\nu})$, where $\delta h=h-h_c$ defines the quantum detuning parameter from the critical coupling h_c and ν is the correlation length exponent. In Fig. 4 *A* and *B*, we present the universal scaling functions $\tilde{\lambda}_{\text{AFM/VBS}}$ obtained from a curve collapse analysis using $h_c=0.69(2)$ and $\nu=0.58(1)$.

In the presence of $SO(5)$ symmetry, the AFM and VBS order parameters are expected to share the same anomalous exponent η. We assume the standard scaling form $\chi_{\text{VBS/AFM}}=L^{2-\eta}\tilde{\chi}_{\text{VBS/AFM}}(\delta h L^{1/\nu})$, where $\tilde{\chi}_{\text{VBS/AFM}}$ are the universal scaling functions of the VBS and AFM order parameters. In Fig. 4 *C* and *D*, we depict the universal scaling functions $\tilde{\chi}_{\text{VBS/AFM}}$ using our previous estimates for h_c and ν and the same anomalous exponent $\eta=1.4(1)$. The increased system size and improved methodology used in this work allowed for a more reliable determination of critical exponents compared with the ones appearing in ref. 25.

In the above scaling analysis, we found that curves corresponding to the smallest system sizes deviate from the expected universal curve. These scaling violations are most likely attributed to

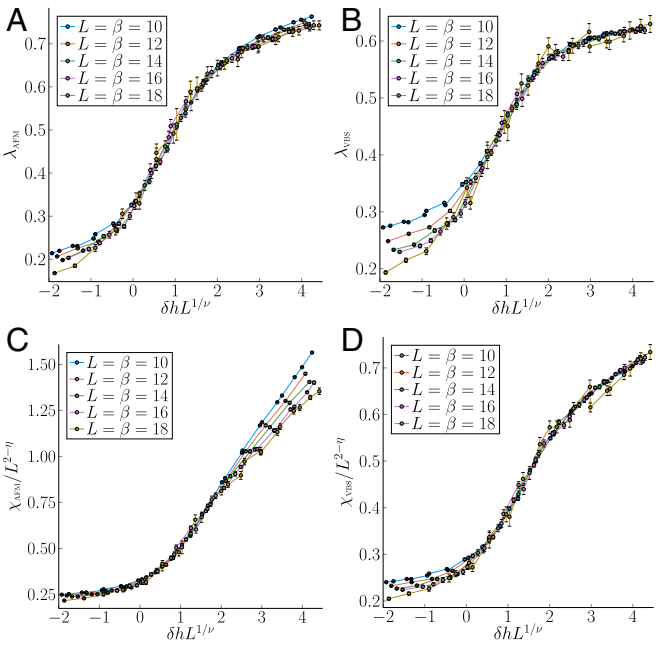

Fig. 4. Finite-size scaling analysis of (*A*) λ_{AFM}, (*B*) λ_{VBS}, (*C*) χ_{AFM}, and (*D*) χ_{VBS}. In all cases, curve collapse is obtained using the critical coupling $h_c=0.69$ and the correlation length exponent $\nu=0.58$. The same anomalous exponent $\eta=1.4$ is used to scale both the AFM and VBS fluctuations.

nonuniversal corrections to scaling that may be sizable at small system sizes. Nevertheless, we note that the critical regime over which we obtain a nearly perfect curve collapse systematically increases with the systems size.

We note that, although the AFM and VBS exponents coincide, the scaling functions, $\tilde{\chi}_{\mathrm{VBS/AFM}}$, in Fig. 4 *C* and *D* do not appear to be the same. The theory to be presented in the section below requires these functions to be the same at leading order, with differences only appearing on considering corrections to scaling. This feature needs to be understood better in future work.

Critical Theory of the Confinement Transition

Previous Work. It is useful to first recall other theories of confinement transitions out of a state with $\mathbb{Z}_2$ topological order (46). The confinement transition of the even ILGT without dynamical matter was already described in the work by Wegner (2), which showed that it was in the (inverted) Ising universality class. The odd ILGT without dynamical matter has a confinement transition to a state with VBS order, and the square lattice critical point is described by a deconfined $U(1)$ gauge theory (5, 7, 47). This can be understood by viewing the $\mathbb{Z}_2$ gauge theory of the topological state as a compact $U(1)$ gauge theory, in which a charge 2 Higgs field has condensed (48). Then, the uncondensing of the Higgs field leads to a confining phase of the $U(1)$ gauge theory across a critical point where the $U(1)$ gauge fields are deconfined: the background $\mathbb{Z}_2$ electric charges of the odd ILGT suppress the $U(1)$ monopoles at the critical point, leading to deconfinement. This furnishes an example of an enlarged gauge group appearing at the confinement–deconfinement critical point of a $\mathbb{Z}_2$ gauge theory. Analogously, we will see that, for our problem of confinement of ILGT coupled to massless fermions, enlarging the gauge group can account for this transition as well. However, here we will need to introduce an $SU(2)$ gauge symmetry as described below.

Fractionalization and Higgs Field: Parton Construction. The f fermions that appear in the Ising gauge theory can be constructed via the following "parton" construction by fractionalizing the physical gauge-invariant degrees of freedom. Notice that the gauge-invariant operators in that model are purely bosonic and include the spin **S** and psuedospin **I** generators. The latter includes the $U(1)$ charge operators I^z and $I^{\pm}$ that create/destroy charged bosons. These can be decomposed into partons as follows. First, define

$$X_r = \begin{pmatrix} f_{r\uparrow} & -f^{\dagger}_{r\downarrow} \\ f_{r\downarrow} & f^{\dagger}_{r\uparrow} \end{pmatrix}. \qquad [4]$$

The spin and psuedospin rotations act via multiplication of $SU(2)$ matrices to the right or left: $X \to U^s X [U^{ps}]^{\dagger}$. Second, the physical operators are

$$\mathbf{S}_r = \frac{1}{4}\,\mathrm{Tr}\left\{X_r^{\dagger}\boldsymbol{\tau} X_r\right\}; \quad \mathbf{I}_r = \frac{1}{4}\,\mathrm{Tr}\left\{X_r \boldsymbol{\mu} X_r^{\dagger}\right\}. \qquad [5]$$

Here, we are using the convention for spin/pseudospin Pauli matrices $\boldsymbol{\tau}/\boldsymbol{\mu}$ from Eq. **3**. Clearly, there is a $\mathbb{Z}_2$ gauge redundancy in this definition corresponding to changing the sign of the fermion operators. Thus, a minimal parton Hamiltonian will have hopping of f fermions mediated by an Ising ($\mathbb{Z}_2$) gauge field as in to our starting model. However, to accomplish the observed transition, we will need a different set of variables. To this end, define a fermion matrix field Y_r, which is superficially similar to the X_r above but only carries the spin quantum number. The psuedospin is assumed to be carried by a triad of bosonic matrix fields $\hat{H}_a$, $a = 1, 2, 3$, each of which is a 2×2 matrix. This can also be written as $\hat{H}_a = \sum_{b=1}^{3} H_{ab}\mu^b = \vec{H}_a \cdot \vec{\mu}$. In terms of these fields, we can decompose the physical operators as

$$\mathbf{S}_r = \frac{1}{4}\,\mathrm{Tr}\{\,Y_r^{\dagger}\boldsymbol{\tau} Y_r\}; \quad I_{ar} = \frac{1}{4}\,\mathrm{Tr}\{\,Y_r \hat{H}_{ar} Y_r^{\dagger}\}. \qquad [6]$$

While spin rotations are implemented as before $Y \to U^s Y$, psuedospin rotations only act on $\hat{H}^a$, which transforms as a vector. This decomposition, however, has additional gauge freedom; for instance, we can simultaneously rotate

$$Y_r \to Y_r\,[U_r^g]^{\dagger}; \quad \hat{H}_{ar} \to U_r^g \hat{H}_{ar}\,[U_r^g]^{\dagger}, \qquad [7]$$

which leaves the physical operators invariant. Therefore, this decomposition has an $SU(2)$ gauge redundancy. Therefore, the effective theory will now involve Y fermions coupled to an $SU(2)$ gauge field. We can readily recover the $\mathbb{Z}_2$ Dirac phase as follows. Consider a Higgs transition, in which the fields H_{ab} acquire an expectation value:

$$\langle H_{ab}\rangle = H_0 \delta_{ab}\,. \qquad [8]$$

Then, $\hat{H}_a = H_0 \mu^a$, and Eq. **6** reduces to Eq. **5**. We will later see that the dynamics at the transition will naturally favor such a Higgs condensate.

Fractionalization and Higgs Field: Rotating Reference Frame Construction. An alternate derivation of the fractionalized degrees of freedom can be obtained by first expanding the Hilbert space of the model to include electron excitations c_α. We can then show that the AFM and VBS order parameters of the possible confining phases and the orthogonal fermions f_α of the $\mathbb{Z}_2$ deconfined phase all emerge by transforming the underlying gauge-invariant electrons, c_α, to a rotating reference frame under $SU_c(2)$.

A similar approach was adopted in refs. 49 and 50, which considered phases with $\mathbb{Z}_2$ topological order in which there are dynamical fermions carrying $\mathbb{Z}_2$ gauge charges and the global $U_c(1)$ charge [$U_c(1)$ is a subgroup of $SU_c(2)$], but these fermions are spinless under $SU_s(2)$. The transition of these phases to confining Fermi liquids (which can be unstable to superconductivity) was described by embedding the $\mathbb{Z}_2$ gauge theory in an $SU(2)$ gauge group. This larger gauge group was needed for a proper description of the confining phase in terms of composites of the fractionalized degrees of freedom (51). It was introduced by transforming to a "rotating reference frame" under $SU_s(2)$. In the topological phase, the $SU(2)$ gauge invariance was broken down to $\mathbb{Z}_2$ by condensing an $SO(3)$ Higgs field, which was neutral under $U_c(1)$ and $SU_s(2)$.

In our case, we transform to a rotating reference frame under $SU_c(2)$ by writing (52, 53)

$$\begin{pmatrix} c_{r,\uparrow} \\ c^{\dagger}_{r,\downarrow} \end{pmatrix} = R_r \begin{pmatrix} f_{r,\uparrow} \\ f^{\dagger}_{r,\downarrow} \end{pmatrix}, \qquad [9]$$

where R_r is a position and time-dependent $SU(2)$ matrix that performs the transformation to a $SU_c(2)$ rotating reference frame. This definition immediately introduces an $SU_g(2)$ gauge invariance, because the right-hand side is invariant under

$$R_r \to R_r\, U_r^g, \quad \begin{pmatrix} f_{r,\uparrow} \\ f^{\dagger}_{r,\downarrow} \end{pmatrix} \to [U_r^g]^{\dagger} \begin{pmatrix} f_{r,\uparrow} \\ f^{\dagger}_{r,\downarrow} \end{pmatrix}, \qquad [10]$$

where U_r^g is an arbitrary space–time-dependent $SU_g(2)$ matrix as in Eq. **6**. The definition in Eq. **9** shows that R_r transforms

as a $SU_c(2)$ fundamental under left multiplication and a $SU_g(2)$ fundamental under right multiplication. Note that, in this $SU_g(2)$ gauge theory formulation and unlike the $\mathbb{Z}_2$ gauge theory in Eq. **2**, at this point the f fermions do not carry an $SU_c(2)$ charge; they only carry an $SU_g(2)$ charge, and the $SU_c(2)$ charge has been transferred from the f to the R.

We now want to obtain an OSM state, proximate to confining AFM/VBS states, from the $SU_g(2)$ gauge theory defined by Eq. **9**. Condensing the R boson would put the $SU_g(2)$ gauge theory in a Higgs phase with no residual gauge invariance, and therefore, we assume that R remains gapped across the transition. However, we can break $SU(2)$ down to $\mathbb{Z}_2$ by condensing a matrix Higgs field, H_{ab}, which is composed of a pair of R bosons:

$$H_{ab} \sim \mathrm{Tr}\left(\mu^a R\, \mu^b R^\dagger\right), \qquad [11]$$

where $a, b = 1, 2, 3$. This is an alternative interpretation of the Higgs field H_{ab} introduced above. Eq. **11** is the analog of the paired condensate of "slave" bosons carrying $U(1)$ gauge charges in the OM construction of ref. 26. H_{ab} transforms as spin 1 under the $SU_g(2)$ gauge and $SU_c(2)$ pseudospin symmetries via left and right multiplications, respectively.

Now introducing a Higgs condensate as in Eq. **8** breaks the gauge $SU_g(2)$ down to $\mathbb{Z}_2$. It also ties together the global $SU_g(2) \times SU_c(2)$ transformations to a diagonal subgroup, so that the f fermions effectively acquire an $SU_c(2)$ index. These are precisely the characteristics of the observed OSM phase.

We note that the Higgs field in Eq. **11** is the only possible R pair without spatial gradients. Other possibilities for R pair Higgs fields are either trivial [$\mathrm{Tr}\left(RR^\dagger\right) = 2$] or vanish identically [$\mathrm{Tr}\left(\mu^a RR^\dagger\right) = \mathrm{Tr}\left(R\,\mu^b R^\dagger\right) = 0$]. We can also make Higgs fields from pairs of the f fermions as was done recently in ref. 54. Such Higgs fields carry only $SU_g(2)$ charges, and their condensation leads to topologically ordered phases with fermionic excitations with global $SU_s(2)$ charges only: these are not orthogonal fermions, and therefore, condensation of the f pair Higgs field does not lead to an OSM.

Critical Theory. We can now write down a continuum theory for a phase transition out of the OSM phase by assembling the degrees of freedom described above in an $SU_g(2)$ gauge theory. We take the continuum limit of the $(f_\uparrow, f_\downarrow^\dagger)$ fermions moving in a π-flux background to obtain two-components Dirac spinors, ψ_v, which carry a valley index $v = 1, 2$ and a fundamental $SU_g(2)$ gauge charge (index not explicitly displayed). The fermions also carry an $SU_s(2)$ charge, but the action is clearer in a Majorana fermion representation (18, 54). Minimally coupling these fermions to an $SU_g(2)$ gauge field, we obtain two-color QCD coupled to $N_f = 2$ flavors of Dirac fermions in three space–time dimensions. This theory was examined recently by Wang et al. (18), and following them, we dub it $\mathrm{QCD}_3(N_f = 2)$.

Wang et al. (18) noted that $\mathrm{QCD}_3(N_f = 2)$ has a global $SO(5)$ symmetry and that a gauge-invariant fermion bilinear transforms as an $SO(5)$ vector. Tracing this fermion bilinear back to the lattice fermions, f_α, they noted that this $SO(5)$ order parameter is precisely the composite of the three-component AFM order parameter and the two-component VBS order parameter. A confining phase of QCD_3 is expected to break the $SO(5)$ symmetry, and therefore, we have achieved our aim of writing down a theory that is proximate to confining phases with AFM or VBS order. We have also obtained an understanding of the evidence for $SO(5)$ symmetry in our numerics.

Finally, we combine $\mathrm{QCD}_3(N_f = 2)$ with a phenomenological action for H to obtain our theory for the transition between the OSM and AFM phases:

$$\begin{aligned}\mathcal{S} = \int d^3x \sum_{v=1}^{N_f} \bar{\psi}_v \not{\partial}_a \psi_v - \frac{1}{2}\mathrm{Tr}\left[\left(D_a^H H\right)^T \left(D_a^H H\right)\right] \\ + \frac{1}{2}m^2\ \mathrm{Tr}[H^T H] + \kappa \det H + \frac{1}{4}\lambda\ \mathrm{Tr}[H^T H]^2 \\ + \frac{1}{4}\lambda'\ \mathrm{Tr}[(H^T H)^2] + \frac{1}{4}f_{\mu\nu}^2.\end{aligned} \qquad [12]$$

Here, a_μ^c represents the $SU(2)$ gauge field, and the covariant derivative of the Dirac fermions is defined as $\not{\partial}_a = \gamma_\mu\left(i\partial_\mu + a_\mu^c \tau^c\right)$, where τ^c are the Pauli matrices. Similarly, the covariant derivative of the Higgs field reads $D_a^H = \left(\partial_\mu + a_\mu^c O^c\right)$, where O^c are the generators of $SO(3)$ rotations. Finally, the last term is the standard Maxwell term, with $f_{\mu\nu}^c$ being the nonabelian field strength. Note that all terms in Eq. **12** respect the global $SO(5)$ symmetry.

The transition between OSM and AFM phases is described by tuning the Higgs mass, m^2, as shown in Fig. 5. For negative m^2, the Higgs field is condensed as in Eq. **8**, and we obtain an OSM phase as described above. Note that the ψ_v fermions remain massless even when the Higgs field is condensed. This is because there is no allowed trilinear Yukawa term between the Higgs boson and the fermions; such a Yukawa term is forbidden by $SU_c(2)$ symmetry, as the matrix Higgs field H carries a $SU_c(2)$ charge, while the fermions ψ do not. This feature is in contrast to earlier theories of phases with $\mathbb{Z}_2$ topological order (49, 50, 54), where the Yukawa term was symmetry allowed, and led to a gap in the fermion spectrum when the Higgs field was condensed.

For positive m^2, we can neglect the massive Higgs field, and then, Eq. **12** reduces to $\mathrm{QCD}_3(N_f = 2)$. For sufficiently large N_f, $\mathrm{QCD}_3(N_f)$ defines a deconfined conformal field theory, with nontrivial scaling dimensions that can be computed in a $1/N_f$ expansion. However, it is expected that there is a critical N_f^c, such that for $N_f < N_c$, the theory is confining. The most recent lattice QMC calculation (55) estimates $N_f^c = 4 - 6$. For $N_f = 2$, which is relevant to our case, a clear "chiral" symmetry breaking was observed, corresponding to a breaking of $SO(5)$ symmetry in our language.[†] Therefore, in Eq. **12**, the Higgs transition provides a means to simultaneously drive confinement and symmetry breaking using a single tuning parameter corresponding to the mass squared of the Higgs field. After we are in the *SO*(5)-broken regime, other irrelevant operators (not shown in Eq. **12**) will become important, and we assume that these select the AFM order observed rather than the VBS order.

Finally, we turn to the critical point between the OSM and AFM phases. We assume that this is described by the *SO*(5)-symmetric deconfined critical theory in Eq. **12** after the Higgs mass m^2 has been tuned to its critical value. The idea is that the additional contributions of the critical Higgs modes, when combined with the gapless fermions, are sufficient to suppress the confining effects of the $SU_g(2)$ gauge field. The continuous transition observed in our numerics along with the evidence for global $SO(5)$ symmetry are evidence in support of our proposal.

We note also the cubic term, which is proportional to κ in Eq. **12**. In purely scalar field theories, this would be sufficient to imply a first-order phase transition. However, when combined with

[†] Strictly speaking, the simulated QCD_3 at $N_f = 2$ does not have the full *SO*(5) symmetry on the lattice scale, because the full symmetry is anomalous. In principle, there is a more exotic scenario (18), in which the QCD theory with full *SO*(5) symmetry flows to the continuous Neel to VBS transition (the deconfined quantum critical point), and chiral symmetry breaking happens only when the full *SO*(5) is explicitly broken [for example, to *SO*(3) × *SO*(2)]. Our theory holds even if this scenario is correct, since the full *SO*(5) is already broken in our microscopic model.

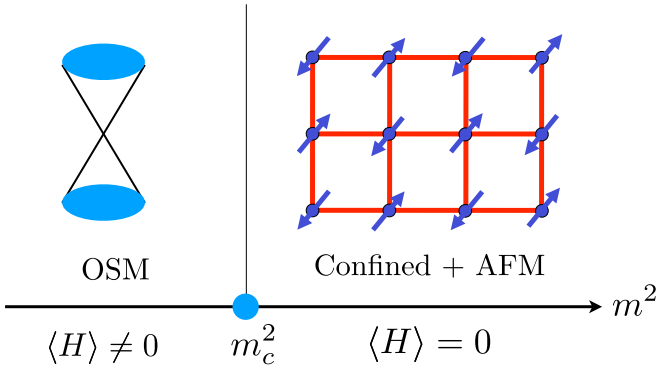

Fig. 5. Higgs mediated confinement transition. For positive Higgs mass, $m^2 > 0$, the Higgs field is gapped. The effective field theory is then QCD_3 ($N_f = 2$), which confines and spontaneously breaks chiral symmetry, leading to an insulator with AFM order. Conversely, for $m^2 < 0$, the Higgs field condenses and reduces the $SU_g(2)$ gauge symmetry down to $\mathbb{Z}_2$, giving rise to the OSM.

strong gauge fluctuations and massless fermions, it is not clear whether estimates that expand about the upper critical dimension can be reliable. In the large-N_f expansion of such a Higgs critical theory (where N_f is the number of fermion flavors), the κ determinant term involves order N_f powers of the Higgs field and is clearly irrelevant at the critical point. Our evidence for a continuous transition is evidence that this is also likely the case at $N_f = 2$.

Even if irrelevant at criticality, on moving into the Higgs phase, the κ determinant term will dictate the nature of the Higgs condensate. Note that, since multiple Higgs fields are present due to the global symmetry, different patterns of Higgs condensates are possible depending on how many $\hat{H}_a$ we condense. These are all degenerate to quadratic order but are differentiated by the determinant term that selects a simultaneous condensate, as in Eq. **8**, independent of the sign of κ. This form of the Higgs condensate is crucial to obtaining the OSM phase.

Discussion and Summary

We have carried out a detailed numerical analysis of the confinement transition of the OSM in a model with a repulsive onsite Hubbard interaction. This serves as a model of a confinement transition in a $\mathbb{Z}_2$ gauge theory coupled to gapless Dirac fermions that carry gauge charge, which is also free of the fermion sign problem. Our key numerical finding is an emergent $SO(5)$ symmetry at criticality that enlarges the microscopic $SO(3) \times C_4$ symmetry associated with spin rotations and the discrete square lattice point group symmetry. Crucially, we show that this result is a qualitatively unique feature of the OSM confinement transition that fundamentally distinguishes it from the more conventional GNY and Ising criticality. In addition, our refined numerical calculations allowed us to improve previous estimates of critical data and further support the scenario of deconfined criticality (DC) with a second-order phase transition.

We note that, even more than a decade after the initial theoretical proposal, the ultimate thermodynamic fate of DC for insulating square lattice antiferromagnets remains in debate. Numerical studies of lattice models show conflicting results, where estimates of certain universal quantities exhibit a significant drift with system size and in certain models, even an indication for a first-order transition. However, several numerical studies indicate an enlarged $SO(5)$ symmetry that is hard to reconcile with a first-order transition (ref. 18 has a recent discussion).

As our model involves fermionic degrees of freedom, its computational cost using standard QMC methodology does not scale favorably with systems size compared with models of non-LGW transitions consisting of bosonic degrees of freedom. It is, therefore, more challenging to assert a strong statement on the thermodynamic limit of our model. Nevertheless, up to the largest length scale studied, we did not observe any sign of deviation from critical scaling, and critical properties seem to remain robust for a wide range of microscopic parameters without any degree of fine tuning. Most relevant for this work, it is difficult to imagine a scenario in which an enlarged symmetry could generically arise at a first-order phase transition.

We used the numerical results as a guide for constructing a field theory description of the OSM confinement transition, which is linked to recent studies of descended phase of $QCD_3(N_f = 2)$ (12, 13, 18, 54). We introduced a matrix Higgs mechanism, which is distinct from the vector Higgs approach presented in ref. 54. In the latter case, the Higgs fields were bilinears of the fermions f_α in contrast to the boson bilinears that we used in Eq. **11**, and their condensation led to spin liquids with fermionic spinons that do not carry the electromagnetic charge. In contrast, condensation of our matrix Higgs field led to an OM, in which the fermions carry both spin and electromagnetic charge. At the same time, the fermions carry $\mathbb{Z}_2$ gauge charge unlike in the SMG scenario of refs. 12 and 13, where a Higgs field in the fundamental representation condenses, giving rise to gapless fermions without gauge charge.

Looking to the future, it would be interesting to explore some extension of our Higgs mechanism. Our QCD_3 mechanism has a natural prediction when time-reversal symmetry is explicitly broken, in which case the Dirac fermions obtain a mass term with total Chern number $C = 2$. Deep in the deconfined phase, this leads to a Semion $\times$ Semion topological order [$\nu = 4$ in Kitaev's 16-fold classification (15)]. However, near the critical point (when the Chern mass scale is greater than the Higgs mass scale), we obtain an $SU(2)_1$ Chern–Simons theory, which is simply the Semion chiral spin liquid. The two topological orders can in principle be distinguished by their ground-state degeneracy on a torus or infinite cylinder, perhaps through density matrix renormalization group calculation. This Semion topological order, if observed, would be a strong signature of the enhanced gauge symmetry near the critical point.

Another extension, which may be implemented in QMC, is to consider similar transitions described by QED_3, namely a $U(1)$ [instead of $SU(2)$] gauge theory coupled to $N_f = 4$ Dirac fermions. There are two scenarios in which this would be natural. One could consider explicitly breaking the pseudospin $SU_c(2)$ symmetry down to $U(1)$, say by breaking the PH symmetry. Alternatively, one can study a similar system but with $\mathbb{Z}_4$ gauge field on the lattice—in fact, in this scenario, we can have more controlled arguments about the ultimate IR fate of the phases and phase transition as we briefly outline in *SI Appendix*. In both cases, the gauge symmetry can be naturally enlarged to $U(1)$ but not $SU(2)$. At the critical point of such QED_3–Higgs transition, we expect an enlarged $SO(2) \times (SO(6) \times U(1))/\mathbb{Z}_2$ symmetry instead of $SO(3) \times SO(5)$ in the QCD_3–Higgs transition [the Neel–VBS $SO(5)$ observed in this work is a subgroup of both symmetries].

On the numerical front, we see several exciting future directions. First, identifying observables that can probe the emergent $SU(2)$ gauge fields and matrix Higgs field, H, would allow for direct confirmation of the critical theory in the numerical simulations. Second, the emergence of an $SO(5)$ symmetry at criticality can be further tested by studying certain high-order correlation functions that are required to vanish by symmetry (19). Third, eliminating the observed nonuniversal corrections to scaling requires simulations on larger lattices beyond standard methodologies. In that regard, one promising approach is the Hamiltonian variant of the fermion bag algorithm (56, 57).

Lastly, we note that, since the theory that we simulated, $\mathcal{H}$, does not contain any gauge neutral fermion, it can be thought of as arising from an underlying bosonic theory. It is tempting to conjecture that the associated bosonic description will also be free of the numerical sign problem. Identifying such bosonic lattice models would allow access to significantly larger system sizes and an accurate study of critical properties.

ACKNOWLEDGMENTS. We thank Shubhayu Chatterjee, Tarun Grover, and Mathias Scheurer for valuable discussions: Shubhayu Chatterjee and Mathias Scheurer pointed out that the det H term in Eq. **12** was allowed. S.G. and A.V. thank Mohit Randeria for an earlier collaboration on a related topic. We acknowledge the Gauss Center for Supercomputing (GCS) e.V. (www.gauss-centre.eu/gauss-centre/EN/Home/home_node.html) for funding this project by providing computing time on the GCS Supercomputer SuperMUC at Leibniz Supercomputing Center (www.lrz.de). S.G. was supported by Army Research Office Grant W911NF-17-1-0606 and European Research Council Synergy Grant UQUAM. S.G. and A.V. were supported by National Science Foundation (NSF) Grant DMR-1411343. F.F.A. thanks the Deutsche Forschungsgemeinschaft through Sonderforschungsbereiche 1170 ToCoTronics for financial support. This research was supported by NSF Grant DMR-1664842 (to S.S.). Research at Perimeter Institute is supported by the Government of Canada through Industry Canada and by the Province of Ontario through the Ministry of Research and Innovation. S.S. also acknowledges support from Cenovus Energy at Perimeter Institute. This work was partially performed at the Aspen Center for Physics, which is supported by NSF Grant PHY-1607611, and the Kavli Institute for Theoretical Physics, which is supported by NSF Grant PHY-1125915. A.V. was supported by a Simons Investigator Grant. C.W. was supported by the Harvard Society of Fellows. This research used the Lawrencium computational cluster resource provided by the Information Technology Division at the Lawrence Berkeley National Laboratory, which is supported by Director, Office of Science, Office of Basic Energy Sciences of the US Department of Energy Contract DE-AC02-05CH11231.

1. Senthil T, Vishwanath A, Balents L, Sachdev S, Fisher MPA (2004) Deconfined quantum critical points. *Science* 303:1490–1494.
2. Wegner FJ (1971) Duality in generalized Ising models and phase transitions without local order parameters. *J Math Phys* 12:2259–2272.
3. Wen XG, Wu YS (1993) Transitions between the quantum Hall states and insulators induced by periodic potentials. *Phys Rev Lett* 70:1501–1504.
4. Chen W, Fisher MPA, Wu YS (1993) Mott transition in an anyon gas. *Phys Rev B* 48:13749–13761.
5. Jalabert RA, Sachdev S (1991) Spontaneous alignment of frustrated bonds in an anisotropic, three-dimensional Ising model. *Phys Rev B* 44:686–690.
6. Chubukov AV, Senthil T, Sachdev S (1994) Universal magnetic properties of frustrated quantum antiferromagnets in two dimensions. *Phys Rev Lett* 72:2089–2092.
7. Sachdev S, Vojta M (1999) Translational symmetry breaking in two-dimensional antiferromagnets and superconductors. *J Phys Soc Jpn* 69:1.
8. BenTov Y (2015) Fermion masses without symmetry breaking in two space-time dimensions. *J High Energy Phys* 2015:34.
9. Ayyar V, Chandrasekharan S (2016) Origin of fermion masses without spontaneous symmetry breaking. *Phys Rev D* 93:081701.
10. Catterall S (2016) Fermion mass without symmetry breaking. *J High Energy Phys* 2016:121.
11. He YY, et al (2016) Quantum critical point of Dirac fermion mass generation without spontaneous symmetry breaking. *Phys Rev B* 94:241111.
12. You YZ, He YC, Xu C, Vishwanath A (2018) Symmetric fermion mass generation as deconfined quantum criticality. *Phys Rev X* 8:011026.
13. You YZ, He YC, Vishwanath A, Xu C (2018) From bosonic topological transition to symmetric fermion mass generation. *Phys Rev B* 97:125112.
14. Senthil T, Fisher MPA (2000) $\mathbb{Z}_2$ gauge theory of electron fractionalization in strongly correlated systems. *Phys Rev B* 62:7850–7881.
15. Kitaev A (2006) Anyons in an exactly solved model and beyond. *Ann Phys* 321:2–111.
16. Tanaka A, Hu X (2005) Many-body spin berry phases emerging from the π-flux state: Competition between antiferromagnetism and the valence-bond-solid state. *Phys Rev Lett* 95:036402.
17. Senthil T, Fisher MPA (2006) Competing orders, nonlinear sigma models, and topological terms in quantum magnets. *Phys Rev B* 74:064405.
18. Wang C, Nahum A, Metlitski MA, Xu C, Senthil T (2017) Deconfined quantum critical points: Symmetries and dualities. *Phys Rev X* 7:031051.
19. Nahum A, Serna P, Chalker JT, Ortuño M, Somoza AM (2015) Emergent SO(5) symmetry at the Néel to valence-bond-solid transition. *Phys Rev Lett* 115:267203.
20. Suwa H, Sen A, Sandvik AW (2016) Level spectroscopy in a two-dimensional quantum magnet: Linearly dispersing spinons at the deconfined quantum critical point. *Phys Rev B* 94:144416.
21. Karthik N, Narayanan R (2017) Flavor and topological current correlators in parity-invariant three-dimensional QED. *Phys Rev D* 96:054509.
22. Sato T, Hohenadler M, Assaad FF (2017) Dirac fermions with competing orders: Non-Landau transition with emergent symmetry. *Phys Rev Lett* 119:197203.
23. Sreejith GJ, Powell S, Nahum A (2018) Emergent SO(5) symmetry at the columnar ordering transition in the classical cubic dimer model. arXiv:1803.11218.
24. Assaad FF, Grover T (2016) Simple fermionic model of deconfined phases and phase transitions. *Phys Rev X* 6:041049.
25. Gazit S, Randeria M, Vishwanath A (2017) Emergent Dirac fermions and broken symmetries in confined and deconfined phases of Z_2 gauge theories. *Nat Phys* 13:484–490.
26. Nandkishore R, Metlitski MA, Senthil T (2012) Orthogonal metals: The simplest non-Fermi liquids. *Phys Rev B* 86:045128.
27. Zhang S (1990) Pseudospin symmetry and new collective modes of the Hubbard model. *Phys Rev Lett* 65:120–122.
28. Auerbach A (2012) *Interacting Electrons and Quantum Magnetism* (Springer Verlag, New York).
29. Kogut JB (1979) An introduction to lattice gauge theory and spin systems. *Rev Mod Phys* 51:659–713.
30. Affleck I, Marston JB (1988) Large-n limit of the Heisenberg-Hubbard model: Implications for high-T_c superconductors. *Phys Rev B* 37:3774–3777.
31. Kitaev A (2003) Fault-tolerant quantum computation by anyons. *Ann Phys* 303:2–30.
32. Wen XG (2002) Quantum orders and symmetric spin liquids. *Phys Rev B* 65:165113.
33. Herbut IF, Juričić V, Vafek O (2009) Relativistic Mott criticality in graphene. *Phys Rev B* 80:075432.
34. Assaad FF, Herbut IF (2013) Pinning the order: The nature of quantum criticality in the Hubbard model on honeycomb lattice. *Phys Rev X* 3:031010.
35. Parisen Toldin F, Hohenadler M, Assaad FF, Herbut IF (2015) Fermionic quantum criticality in honeycomb and π-flux Hubbard models: Finite-size scaling of renormalization-group-invariant observables from quantum Monte Carlo. *Phys Rev B* 91:165108.
36. Otsuka Y, Yunoki S, Sorella S (2016) Universal quantum criticality in the metal-insulator transition of two-dimensional interacting Dirac electrons. *Phys Rev X* 6:011029.
37. Sachdev S, Morinari T (2002) Strongly coupled quantum criticality with a Fermi surface in two dimensions: Fractionalization of spin and charge collective modes. *Phys Rev B* 66:235117.
38. Assaad F, Evertz H (2008) *World-Line and Determinantal Quantum Monte Carlo Methods for Spins, Phonons and Electrons*, eds Fehske H, Schneider R, Weisse A (Springer, Berlin), pp 277–356.
39. Bercx M, Goth F, Hofmann JS, Assaad FF (2017) The ALF (Algorithms for Lattice Fermions) project release 1.0. Documentation for the auxiliary field quantum Monte Carlo code. *SciPost Phys* 3:013.
40. Pujari S, Lang TC, Murthy G, Kaul RK (2016) Interaction-induced Dirac fermions from quadratic band touching in bilayer graphene. *Phys Rev Lett* 117:086404.
41. Polyakov AM (1978) Thermal properties of gauge fields and quark liberation. *Phys Lett B* 72:477–480.
42. Isakov SV, Hastings MB, Melko RG (2011) Topological entanglement entropy of a Bose-Hubbard spin liquid. *Nat Phys* 7:772–775.
43. Grover T, Zhang Y, Vishwanath A (2013) Entanglement entropy as a portal to the physics of quantum spin liquids. *New J Phys* 15:025002.
44. Fredenhagen K, Marcu M (1986) Confinement criterion for QCD with dynamical quarks. *Phys Rev Lett* 56:223–224.
45. Gregor K, Huse DA, Moessner R, Sondhi SL (2011) Diagnosing deconfinement and topological order. *New J Phys* 13:025009.
46. Sachdev S (2018) Topological order and Fermi surface reconstruction. arXiv:1801.01125.
47. Senthil T, Balents L, Sachdev S, Vishwanath A, Fisher MPA (2004) Quantum criticality beyond the Landau-Ginzburg-Wilson paradigm. *Phys Rev B* 70:144407.
48. Fradkin E, Shenker SH (1979) Phase diagrams of lattice gauge theories with Higgs fields. *Phys Rev D* 19:3682–3697.
49. Sachdev S, Chowdhury D (2016) The novel metallic states of the cuprates: Fermi liquids with topological order and strange metals. *Prog Theor Exp Phys* 2016:12C102.
50. Chatterjee S, Sachdev S, Scheurer M (2017) Intertwining topological order and broken symmetry in a theory of fluctuating spin density waves. *Phys Rev Lett* 119:227002.
51. Sachdev S, Metlitski MA, Qi Y, Xu C (2009) Fluctuating spin density waves in metals. *Phys Rev B* 80:155129.
52. Lee PA, Nagaosa N, Wen XG (2006) Doping a Mott insulator: Physics of high-temperature superconductivity. *Rev Mod Phys* 78:17–85.
53. Xu C, Sachdev S (2010) Majorana liquids: The complete fractionalization of the electron. *Phys Rev Lett* 105:057201.
54. Thomson A, Sachdev S (2018) Fermionic spinon theory of square lattice spin liquids near the Néel state. *Phys Rev X* 8:011012.
55. Karthik N, Narayanan R (2018) Scale-invariance and scale-breaking in parity-invariant three-dimensional QCD. *Phys Rev D* 97:054510.
56. Huffman E (2016) Monte Carlo methods in continuous time for lattice Hamiltonians. arXiv:1611.01680.
57. Huffman E, Chandrasekharan S (2017) Fermion bag approach to Hamiltonian lattice field theories in continuous time. *Phys Rev D* 96:114502.